Fast Spectroscopy of Laser-Initiated Nanoenergetic Materials

Yanqiang Yang, Zhaoyong Sun, Shufeng Wang, and Dana D. Dlott*

School of Chemical Sciences, Box 01-6 CLSL, 600 South Mathews Avenue, Urbana, Illinois 61801

Received: September 6, 2002; In Final Form: March 4, 2003

Nanoenergetic materials consisting of aluminum nanoparticle (50−200 nm) aggregates termed ALEX plus nitrocellulose (NC) oxidizer are studied by ultrafast spectroscopy following 100 ps laser flash-heating. Thermal conduction calculations are used to estimate the initial ALEX temperature as a function of laser fluence, and to show that initiation and ignition occurs as a result of the reaction between nearly uniformly heated ALEX particles and cold NC. The onset of light emission and Al oxidation occurs near the melting point of Al, and fast violent ignition reactions begin near the vaporization transition. At lower fluences and lower ALEX concentrations, hot spots consisting of an ALEX aggregate and nearby NC ignite and then die out. At higher fluences and higher ALEX concentrations, the ignition reaction propagates from the hot spots throughout the entire laser-heated region. The nanosecond-duration burst of light accompanying ignition triggered by vaporizing ALEX consists of a continuum peaked near 500 nm plus features associated with electronically excited Al atoms and hot excited AlO. The time for energy release with high-temperature initiation and minimal contribution from mass transport is ∼2 ns. When the ignition reaction also propagates through the sample, the time for energy release is increased. Coherent anti-Stokes Raman (CARS) measurements of nitro consumption via the disappearance of ONO_2 (nitrato) groups of the NC due to Al attack on the oxidizer show two distinct phases of ∼300 ps and ∼2 ns, associated with hot spot initiation and propagation, respectively. The 300 ps time constant for nitro consumption adjacent to an Al particle is significantly shorter than the 2 ns time constant for energy release. The rate-limiting step in energy release is neither nanoparticle depassivation nor oxidization chemistry, but rather is nonradiative relaxation of hot molecules produced by Al oxidation.

1. Introduction

Energetic materials containing nanometer Al particles,[1,2] which can release more than twice as much energy as the best molecular explosives,[3,4] have recently become a subject of intense interest. Compared to "conventional" formulations that use Al particles typically 30 μm average diameter with a broad size distribution,[5] nanomaterials offer the possibility of faster energy release, more complete combustion and greater control over performance. A lack of understanding of the fundamental mechanisms has hindered the development of nanoenergetic materials. With conventional particles, chemistry is mainly limited by mass transport.[5] The time for reaction in the diffusion regime is proportional to the particle diameter d^2.[6] As the particle size is reduced, the d^2 behavior will eventually break down as diffusion-controlled processes become comparable in rate to chemical reactions. In that limit chemical dynamics would be expected to play a more significant and possibly dominant role. In previous work,[7] we used picosecond laser flash heating to investigate a model nanoenergetic material, consisting of a commercially available Al nanoparticle aggregates[8] termed ALEX, 1 wt % in an oxidizing nitrocellulose (NC; 12% N) binder (Figure 1a). According to the manufacturer, ALEX from Argonide Corp. (Sanford, FL) consists of micron-scale aggregates of 50−200 nm spherical particles. The surface area is ∼15 m^2/g. The surface is passivated[9] with a native oxide layer. ALEX contains 70−80% zerovalent Al. After the ALEX particles were flash-heated[7] to the vaporization temperature, 2740 K, time-resolved emission and time-resolved coherent anti-Stokes Raman scattering (CARS) were used to study chemical reaction initiation and fast energy release. A 5 (±2) ns burst of emission was observed. CARS measurements of nitro consumption due to Al attack on the oxidizer occurred on the 300 ps time scale. Because Al oxidization was so much faster than energy release, as indicated by the 5 ns duration of the emission burst, we suggested that the rate-limiting process in

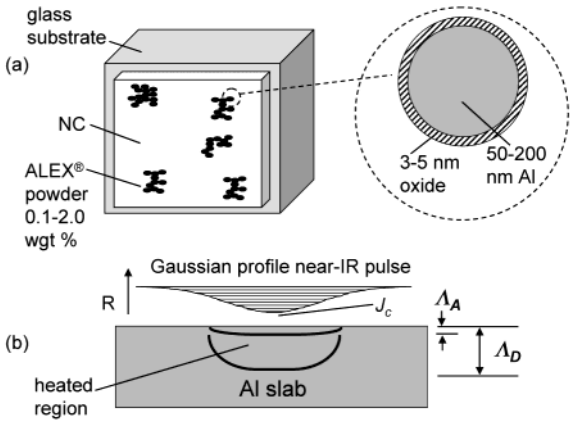

Figure 1. (a) Nanoenergetic samples are a suspension of aluminum nanoparticles termed ALEX in nitrocellulose (NC) thin film on a glass substrate. A near-IR pulse flash-heats the ALEX particles. ALEX consists of micron-scale aggregates of 50−200 nm spherical particles. Each sphere (inset) is passivated by a 3−5 nm thick oxide. (b) Laser heating calculations assume a metal slab of reflectivity R irradiated by a near-IR pulse. J_c is the fluence at the center of the Gaussian radial profile. The pulse is absorbed in a layer of thickness Λ_A, but the sample is heated to a depth Λ_D, where Λ_D is the thermal diffusion length during the pulse.

* To whom correspondence should be addressed. Phone: 217-333-3574. Fax: 217-244-3186. E-mail: dlott@scs.uiuc.edu.

10.1021/jp0269322 CCC: $25.00
Published on Web 04/19/2003

energy release was not chemistry but nonradiative relaxation of hot nascent oxidized Al molecules such as AlO.[7]

In this paper we present a more complete description of the dynamics of laser ignition of ALEX/NC nanoenergetic composites. Detailed laser-fluence and concentration-dependence studies are reported. Optical microscopy is used to help understand the spatial propagation of initiation and ignition reactions, and the spectroscopic measurements have improved temporal and spectral resolution.

With molecular high explosives such as the most widely used high-performance explosive HMX (octahydro-1,3,5,7-tetranitro-1,3,5,7-tetraazacine, $C_4H_8N_8O_8$),[10] each molecule contains both fuel and oxidizer. The heat of explosion[10] of HMX is $\Delta H_{expl} = 11.1$ kJ/cm^3. A few experimental explosives such as[11] CL20 and octanitrocubane[12,13] are perhaps 30% more powerful. After fast heating or shock initiation, molecular explosives break down endothermically into smaller fragments creating a reactive stew.[14] Energy is released as a result of just a few highly exothermic recombination reactions that are the culmination of a long chain of events.[14−16] An estimate of the maximum energy release rate in HMX is obtained from detonation experiments[14] involving high temperatures and pressures of about 4000 K and 40 GPa.[10,17−19] The reaction zone is 0.1−1.0 mm wide behind the HMX detonation front propagating at 9 mm/μs, so energy release occurs on the 10−100 ns time scale.[14] The rate-limiting process in energy release is chemistry—generating the lowest energy molecules out of the reactive stew.

"Nonideal" is a term sometimes used for energetic materials with separate fuel and oxidizer, which can be ignited or shock-initiated. The materials studied here actually consist of three parts, the fuel particles, their associated passivation layer, and the oxidizer. At low heating rates, these materials can be ignited when they reach the melting point, $T_m = 933$ K for Al,[5] where the metal passivation layer starts to break down and the metal becomes active to reaction with the oxidizer. Detonation or high-temperature propellant combustion are associated with high heating rates and high temperatures[10] up to perhaps 4000 K, so depassivation might be a more dynamic process associated with Al reaching the vaporization temperature $T_{vap} = 2740$ K. The gas-phase thermochemistry[20] of Al has been studied experimentally and theoretically,[3,4] but little is known about the condensed-phase chemistry. In aluminum−oxygen systems, it is believed that AlO forms first,[21] but many other species are typically present,[3,4] such as Al_2O and AlO_2. The final lowest-energy state is condensed-phase (usually liquid) Al_2O_3,[5] which is formed by a variety of reactions including $AlO + AlO_2$. Most or all Al oxidation reactions are exothermic, and some generate extremely hot nascent molecules that are electronically excited with high levels of vibrational excitation. Some of the most exothermic compositions suitable for nanoenergetic materials include[1] Al + MoO_3 (16 kJ/cm^3) and Al + PTFE (poly(tetrafluoroethylene)) (theoretical value 22 kJ/cm^3). In conventional Al explosives, Al_2O_3 has been observed to form at rates of micrometer per microsecond, which is indicative of energy release in ~100 μs, about 10^3 times slower than in HMX. ALEX propellants have been observed to burn more than 20 times[8,22,23] as fast as conventional Al, and Argonide Corp. suggests that an ALEX particle can be consumed in less than 100 ns. A propellant with an ALEX/NC base (15% ALEX) was observed[22] to produce 10 kJ/cm^3. Flash-heating emission studies of a different nanoenergetic material, 500 nm Al with PTFE (Teflon AF) oxidizer were reported by Parker et al.[24] The initiation pulse duration was 8 μs and the apparatus time resolution was 1.25 μs. The 500 nm Al particles were believed consumed on the 6 μs time scale.

In our flash-heating experiments, a 100 ps duration, 1.053 μm near-infrared (near-IR) laser pulse initiates the explosive by heating the metal particles almost uniformly to a high temperature.[7] The ALEX/NC composite is fabricated into a film a few microns thick on a large-area glass or silica substrate. Tiny sample volumes typically 150 μm in diameter, weighing about 50 ng, are initiated and probed at a high repetition rate (typically 80 Hz). A motorized positioner ensures that each pulse hits a fresh spot. With the exception of the high-resolution emission measurements described later, the nanoparticle concentration in our samples was kept low to allow optical access to the interior of the samples. On the basis of oxygen balance[10] we find that to produce Al_2O_3, a stoichiometric sample should be 32% Al and 68% NC (12%N) by weight, whereas our samples were typically 0.1−2.0% ALEX by weight.

The principal focus of the present work is determining the rates and mechanisms of processes widely discussed in the energetic materials community:[10,25] *initiation, ignition, hot spot formation, propagation, and energy release*. *Initiation* refers to the onset of widespread chemical reactions. *Ignition* refers to the onset of widespread reactions that produce large amounts of heat and light. *Energy release* occurs immediately after ignition. Depending on which processes limit the rate of *energy release*, ignition could be much slower than initiation. When a nanoparticle and its surrounding oxidizer shell are ignited, a laser-generated *hot spot* is formed. Hot spots are frequently discussed in the explosives literature, and low velocity initiation of most solid explosives begins at hot spots.[26,27] Depending on the size, the temperature, and a variety of other parameters, a hot spot might grow or it might extinguish.[28,29] If a hot spot grows, or if there are many nearby hot spots that interact, the ignition reaction can *propagate* throughout the explosive, causing complete ignition.

On the basis of this discussion, we can put forth a plausible scenario[7] for our flash-heating experiments that forms a context for a critical analysis of our data. (1) The passivation layer breaks down, activating the flash-heated particles. (2) Hot Al metal attacks the NC surrounding each ALEX aggregate. (3) The possible chemistry is too complicated to catalog, so we will focus primarily on the creation of AlO, the dominant emitting species in the visible, resulting from reactions of Al with ONO_2 (nitro). AlO as well as other species containing Al will be produced with extensive levels of vibrational and electronic excitation. (4) These hot molecules release a burst of light and heat that indicates hot spot ignition. (5) The ignition reaction can propagate into the NC between the ALEX aggregates. NC is an energetic self-oxidizing polymer with a heat of explosion (12% N) of 5.7 kJ/cm^3.[10] (6) Even if the ignition reaction spreads throughout the flash-heated volume, it will not continue to spread over distances larger than the sample thickness (2−3.5 μm) due to heat loss at the substrate and air interfaces. This scheme may be summarized as follows:[7] flash heating of Al → activation/depassivation → oxidizer attack → hot nascent species → radiative and nonradiative energy release → propagation → termination.

2. Temperature Calculations for Laser Flash Heating

Standard techniques are available for calculating the temperature of a metal surface heated by laser pulses,[30] and for calculating the shock wave generated by a spherical particle embedded in a fluid medium.[31] The problem is that we do not yet have a good way of determining the absorbance of the ALEX

nanoaggregates in suspension and its dependence on size and shape. Given these uncertainties, rather than attempting a detailed hydrodynamic model we will generate rough estimates of particle temperature and pressure as a function of flash-heating fluence, recognizing there will be a broad distribution of T and P due to random properties of the nanoaggregates. We will then assess the accuracy of this model by looking for changes in the emission and chemical reactivity near the predicted fluence thresholds for melting and boiling. Of course it helps that the aluminum temperature becomes independent of fluence at the transition temperatures.

Figure 1b shows a metal slab irradiated by a near-IR laser beam with a Gaussian radial profile. The radial dependence of the fluence $J(r)$ for a pulse with energy E_P is

$$J(r) = \frac{2E_P}{\pi w_0^2} \exp\left(-\frac{2r^2}{w_0^2}\right) \quad (1)$$

where w_0 is the beam radius.[32] The fluence at the beam center is denoted J_c. Equation 1 shows that $J_c = 2E_p/\pi\omega_0^2$. The CARS probe beams interrogate a 50 μm diameter region at the center of the 140 μm diameter flash-heating beam, where the fluence is uniform to $\pm$11%.[33] We will refer to this 50 μm diameter region as the "heated region". The emission intensity is highly sensitive to fluence, so most of the emitted light comes from the hottest regions at the beam center. Whenever we cite a fluence for the flash-heating pulse, we mean J_c. Notice J_c is twice the average fluence $E_p/\pi\omega_0^2$.

Near-IR light on an oxidized Al surface is absorbed within a thin layer of thickness $\Lambda_A \approx 3$ nm, where it is instantly converted to heat.[34] At the end of a pulse of duration t, the slab will be heated to a depth equal to the thermal diffusion length[30] $\Lambda_D(t)$, provided $\Lambda_D(t) \gg \Lambda_A$. The thermal diffusion length is given by

$$\Lambda_D(t) = \frac{1}{2}\sqrt{2\pi Dt} \quad (2)$$

where $D = \kappa/\rho C$ is the thermal diffusivity, κ the thermal conductivity, ρ the density, and C is the heat capacity. For Al metal, $D = 10$ cm^2/s.[35]

In the composite materials used here (Figure 1a), the near-IR pulse is absorbed only by the metal particles. There are actually three distinct time scales for heat flow (vide infra): the time for heat to spread uniformly through the metal particle (100 ps), the time for heat to spread through the polymer matrix (a few microeconds), and the time for heat to escape into the glass substrate (70 μs). If we take the diameter of the individual nanoparticles comprising the ALEX aggregates to be 100 nm, then heat spreads throughout each nanoparticle during the pulse. *Thus a 100 ps that is absorbed only near the surface still heats the Al nanoparticles almost uniformly*. The diffusivity $D = 10^{-3}$ cm^2/s for typical organic polymers[35] including NC. During the 100 ps pulse, thermal diffusion heats only a negligible 4 nm thick shell of NC around the ALEX. If the ALEX particles do not react with the oxidizer, they will cool, heating the surroundings. The cooling process will be nonexponential in time. When the ALEX is much hotter than the surrounding NC, there will be a fast (roughly nanosecond) burst of cooling as heat moves out of the ALEX into a shell of NC a few tens of nanometers thick, but then cooling will slow as heat diffuses into the NC between the particles. The time for the ALEX and NC to come to thermal equilibrium depends on the distance between the hot particles, which is difficult to determine for random aggregates. At the highest and lowest ALEX concentrations used here, 0.1% and 2.0 wt %, the mean distance between 100 nm particles would be 1.3 and 0.5 μm. Equation 2 then says the ALEX and NC will equilibrate in 1.5$-$0 μs. Using 3.3 μm for the film thickness, the time for heat to escape into the substrate is 70 μs.

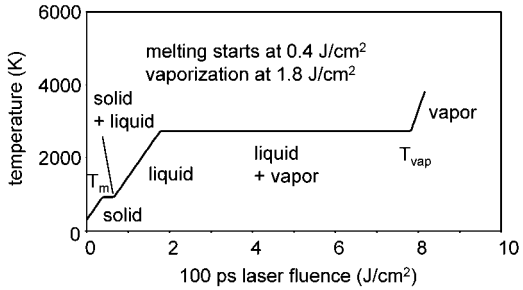

Figure 2. Calculated temperature of aluminum with 100 ps heating pulses at the indicated fluence. T_m and T_{vap} indicate the temperatures of melting and the onset of vaporization.

To calculate the uniform temperature of an ALEX particle immediately following the 100 ps flash-heating pulse, we assume no heat loss to the NC and no significant heat generation by chemical reactions. The absorbed energy per unit volume E_v and the final temperature T_f at the end of the pulse are given by

$$E_v = J(1 - R)\Lambda_D = \rho\int_{T_i}^{T_f} C(T)\, dT \quad (3)$$

where R is the reflection coefficient, $(1 - R)$ is the fraction of incident light absorbed, and $C(T)$ is the heat capacity. For Al, $C(T)$ includes[35] the latent heat of fusion ΔH_f at the melting temperature $T_m = 933$ K and the latent heat of vaporization ΔH_{vap} at the boiling transition ($T_{vap} = 2740$ K at 1 atm). Even though there is be some pressure buildup in the sample, we will regard the 1 atm boiling point of Al as the threshold temperature for significant vapor generation.

We have assumed $R = 0.95$, the known value for bare oxidized Al thin films on glass, which ignores nanoparticle size and scattering effects.[36] Obviously, a small error in R causes a much larger error in $(1 - R)$, and metal nanoparticles might have a very different absorption than bulk metal. Examination of a variety of size-selected spherical Al nanopowders, including particles with mean diameters of 30, 60, and 110 nm obtained from Technanogy, Inc. (Irvine, CA) and 20 μm particles from Aldrich shows that only the 30 nm particles have a different appearance (brown). Major size effects in the absorption of Al nanoparticles evidently occur only below 60 nm. The ALEX aggregates composed of 50$-$200 nm particles have the same metallic gray appearance as the other metal particles.

Figure 2 shows the computed temperature of uniformly heated Al particles as a function of 100 ps flash-heating fluence. The putative fluence at melting $J_m = 0.4$ J/cm^2, and the putative fluence at the vaporization threshold $J_{vap} = 1.8$ J/cm^2. Due to the large ΔH_{vap}, the region of liquid$-$vapor equilibrium is broad, spanning a range of four in fluence.

If the ALEX particles cool and heat the NC without reacting, then the final temperature of the equilibrated ALEX/NC composite (prior to heat loss into the substrate) can be computed using eq 3, where E_v still refers to the energy per unit volume of Al, but the heat capacity is now the combined heat capacity of the Al + NC sample. Figure 3 shows the result over the range of fluences and ALEX concentrations used here. Even at the highest fluence ($J_c = 8.5$ J/cm^2) and the highest Al concentration (2% ALEX), the expected bulk temperature rise

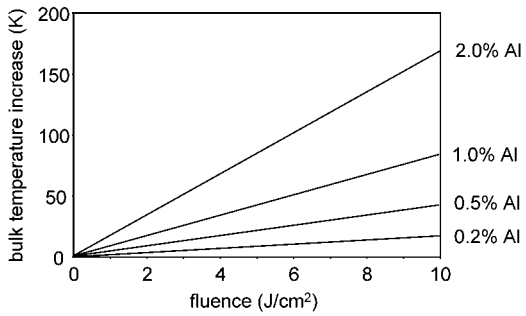

Figure 3. Calculated temperature of Al/NC samples assuming the flash-heated nanoparticles come to equilibrium without reacting with NC. Even at the highest laser fluence with the greatest Al concentration, the bulk temperature increase would not be enough to thermally decompose NC.

is less than 150 K. Significant thermal decomposition of NC does not occur below 200 °C with long-duration heating, and with flash heating about 550 °C is needed.[37] We do not put enough heat into the sample to thermally decompose uniformly heated NC. *The chemistry seen here is primarily a consequence of reactions between high-temperature Al particles and cold NC.*

A pressure jump is generated whenever there is isochoric heating. We will calculate the pressure jump in the absence of metal vapor formation and chemical breakdown of the NC, recognizing this represents a lower limit to the pressure jump. In this case, the pressure jump is $\Delta P \approx (\partial P/\partial T)_V \Delta T$. Similar to the temperature discussion, there are three time scales for relaxation of the pressure jump.[31,38] Volume relaxation of a metal particle occurs at approximately the sound velocity ~5 nm/ps; the approximate time for volume relaxation of a 100 nm nanoparticle of Al is therefore ~20 ps. Thus with 100 ps heating there is hardly any pressure jump within the nanoparticle. For polymers similar to NC absent significant chemistry, the pressure coefficient is approximately 10 atm/deg.[39] Thus the local pressure in the NC shell surrounding each nanoparticle at 2740 K is at least 2.7 GPa. Because a typical shock velocity in the polymer[39,40] is 4 μm/ns, the high-pressure centers near each nanoparticle will equilibrate with the cold NC between the particles within 125−300 ps. At that point, absent chemistry, the bulk sample pressure jump can be determined from Figure 3 to be at most 0.15 GPa (1.5 kB). This bulk sample pressure is released when the rarefaction wave propagates from the free surface to the substrate.[41] For our 3.3 μm films, this occurs in ~800 ps.

3. Experimental Section

The thin film samples on glass substrates were mounted on a motorized *xy* positioner. They were repetitively flash-heated by 100 ps duration 1.053 μm pulses up to 640 μJ in energy, focused to 140 μm diameter, at a repetition rate of 80 Hz (the maximum obtainable $J_c = 8.5$ J/cm^2). The speed of the positioner was adjusted to provide a center-to-center distance between ignited spots of a few beam diameters.

A. Sample Preparation. ALEX from Argonide Corp. and NC from Aldrich (12% nitrogen, viscosity 800−1000 s, Cat. No. 43,505-8) were used without further purification. Thin films were prepared by spin coating an ALEX/NC solution at 600 rpm on a glass or silica substrate. A solvent mixture that produces high-quality thin films was used.[41] It contained methyl ethyl ketone, some higher viscosity ketones, and Pluronic L-62 surfactant (BASF Corp.). The ALEX was added and the mixture sonicated for several minutes to break up any ALEX clumps. Then NC was added to produce a solution 4.8 wt % NC. It worked better to sonicate the ALEX in the lower viscosity solvent before adding the NC. An optical profilometer was used to measure the film thickness.

In experiments where the time-integrated emission was collected, we were concerned about the possibility of long-lived emitting species escaping from the light collection region. We performed most experiments with the sample trapped in a glass sandwich to prevent escape. For CARS or fast PMT experiments, a single sided geometry with no cover glass was used, because we reasoned that the <7 ns duration of the experiment is too short for any sample to escape. The CARS experiments used float-glass soda lime substrates 10 × 10 cm^2. The emission experiments used silica microscope slides because the strongly emitting sodium and potassium in soda-lime glass produced too many extraneous emission lines. In more recent experiments, we have been able to remove the substrate entirely and study the free thin films. No significant differences were observed, showing that effects of one-sided or two-sided substrates were minimal.

B. Emission. Light was collected and collimated by a 5X microscope objective. The collimated light was fed into a 200 μm diameter optical fiber with collection lens. The output of the optical fiber could be routed to a spectrograph with a CCD array, a high resolution $^3/_4$ m CCD spectrograph, or a fast photomultiplier (PMT). The spectrograph monitored the 375−1100 nm range with a resolution of ~4 nm. However, data above 775 nm were contaminated by second-order scattering from the Al atomic emission and were discarded. A calibrated tungsten−halogen lamp showed that the spectral response of the CCD spectrograph combination was nearly flat in the 375−775 nm range, so no correction was used. The high resolution spectrograph had a resolution of better than 0.1 nm, and spectra were also not corrected. The fast PMT (Hamamatsu R5900U-04) simultaneously monitors all emission in the 350−820 nm range. The lower limit is set by the glass optics and the upper limit by the PMT spectral cut off. The PMT oscilloscope system had an impulse response with ~1 ns fwhm (see Figure 8).

C. CARS. The broadband multiplex CARS setup used to monitor the symmetric nitrato stretching transition of NC has been described elsewhere.[33,41,42] The probe pulse duration ~30 ps is significantly shorter than the 100 ps flash-heating pulse. The spectral resolution was ~1 cm^{-1}, and the width of the selected spectral region is ~350 cm^{-1}. Each displayed spectrum or data point was the average of 17 integrations over a 1 s period, corresponding to a total of ~1300 laser shots.

4. Results

A. Morphology. Figures 4 and 5 are visible-light microscope images, obtained using a monochrome camera and computer with video frame grabber, of representative spots after single-shot flash-heating with no cover glass, illustrating the concentration and fluence dependence. In Figure 4, samples with 0.1−2.0% ALEX concentration were irradiated at $J_c = 5.9$ J/cm^2. In Figure 5, samples with 1% ALEX were irradiated with fluences $J_c = 0.4-5.2$ J/cm^2. The circles at the bottom of Figure 4 outline the diameters (1/e^2 intensity circles) of the pump pulse (140 μm), the smaller of the CARS probe pulses (50 μm), and the 50 μm diameter "heated region" at the center of the flash-heating pulse. The black specks in the unexposed region outside the heated region are the occasional larger ALEX aggregate.

Figures 4 and 5 show that at lower fluences and lower ALEX concentrations the ignition reaction is confined to a sprinkling of spots that ignite and extinguish without igniting the entire

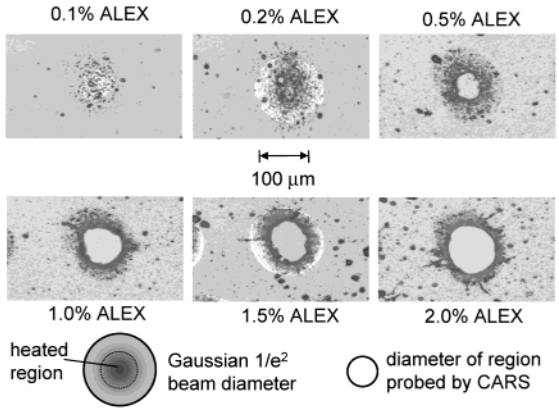

Figure 4. Optical micrographs (monochrome camera) of Al/NC samples 3.3 μm thick exposed to single 100 ps pulses at $J_c = 5.9$ J/cm^2. At lower concentrations, isolated spots are observed, which ignite and extinguish without igniting the entire heated region. Around 0.5% ALEX, a concentration threshold is reached where the entire heated region is consumed. The ignition reaction does not propagate more than a few microns outside the heated region due to heat loss at the substrate interface. The circles below indicate the 140 μm diameter (1/e^2 intensity circle) of the near-IR flash-heating pulse and the 50 μm diameter region probed by CARS. The "heated region" is the central 50 μm of the heating pulse, where the fluence is uniform to ±11%.

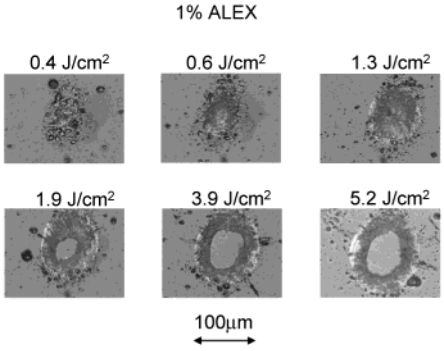

Figure 5. Optical micrographs of Al/NC samples with 1% ALEX by weight, exposed to single pulses at the indicated fluences. The fluence threshold for total ignition of the heated region is just above $J_c = 1.9$ J/cm^2.

heated region. Figure 4 shows that the concentration threshold for total ignition is about 0.5% ALEX with $J_c = 5.9$ J/cm^2. Figure 5 shows that this concentration threshold at 1.0% ALEX is between $J_c = 1.3$ J/cm^2 and $J_c = 1.9$ J/cm^2.

B. Time-Integrated Emission. Figures 6 and 7 show the time-integrated emission resulting from flash-heating. The data in Figure 6a were obtained from a sample with 1% ALEX. However, there was remarkably little difference between spectra at a given fluence obtained with ALEX concentrations throughout the 0.1−46% range, except the overall intensity. The spectrum in Figure 6a at $J_c = 5.2$ J/cm^2 consists of a broad continuum in the 375−775 nm range peaked around 500 nm. On top of this continuum are much weaker features marked (i)−(v). Higher resolution views of (i)−(iv) are shown in the insets. The spectra in the insets were obtained using the high-resolution spectrograph and a sample with 33% Al to generate higher intensities needed to offset poor throughput. Features (i)−(v) correspond to a small amount of structured emission on top of the broad background. On the basis of studies of Al ablation in air,[43] (i) is assigned to the well-known Al atomic emission doublet,[35] and (ii)−(iv) to the well-known blue-green emission of the B → X transition of AlO, corresponding to $\Delta\nu = 1$, 0, and −1 respectively.[21,44−46] Feature (v) is an emission

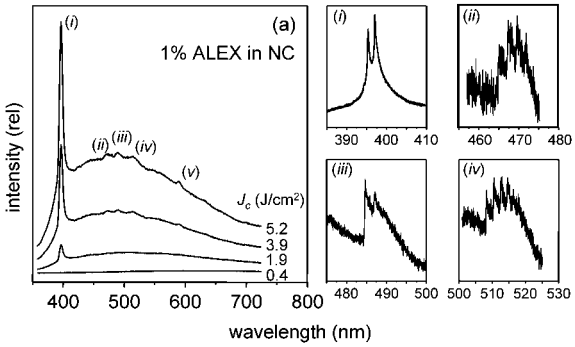

Figure 6. (a) Time-integrated emission spectra from samples with 1.0% ALEX at the indicated fluences. The spectra of the features labeled (i)−(iv), obtained using a sample with 46% ALEX and a high-resolution spectrograph, are shown in the insets at right. These sharp features ride on top of the broad background. (i) is the well-known Al atom emission doublet. (ii)−(iv) are vibronic transitions of hot AlO. (v) is a sodium doublet due to impurities.

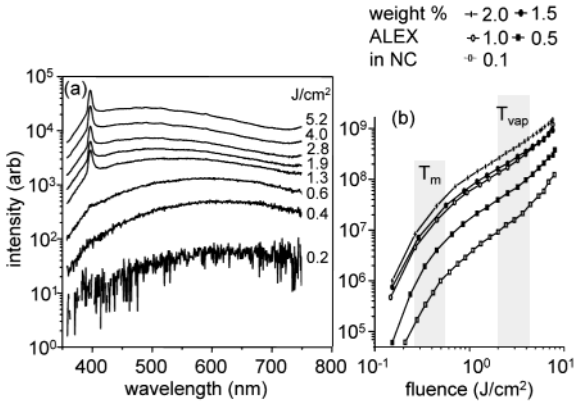

Figure 7. (a) Semilog plot of emission spectra at the indicated fluences (J/cm^2) from 1% ALEX/NC. (b) Total emission intensity as a function of fluence at the indicated ALEX concentrations. The shaded regions indicate where the intensity curves show breaks in slope. The regions labeled T_m and T_{vap} include the predicted fluences for the onset of melting ($J_c = 0.4$ J/cm^2) and vaporization ($J_c = 1.8$ J/cm^2).

doublet from sodium present as an impurity. The high-resolution features in the insets are ordinarily associated with gas-phase spectra. Given the small relative amplitudes, these features most likely arise from reactions in gas pockets or at the air interface.

Figure 7a is a semilog plot of the emission spectrum as a function of laser fluence in a 1% ALEX sample. The structured Al and AlO emissions are associated with higher fluences and they disappear below $J_c = 1.3$ J/cm^2. At still lower fluences at and below $J_c = 0.4$ J/cm^2, the spectrum is weak and unstructured, and the peak shifts to the red with decreasing fluence. This emission is reminiscent of a graybody spectrum (a graybody is a blackbody spectrum with emissivity $\eta < 1$), but proving that would require absolute intensity measurements over a wider wavelength range.[18]

The right-hand side of Figure 7 shows a log−log plot of the fluence dependence of the total emission intensity in the 400−650 nm range. The curves representing different ALEX concentrations run almost parallel, so the ALEX concentration affects mainly the absolute intensity. Each curve evidences two breaks in slope. These breaks in slope are not dramatic, but because this is a log−log plot, the effect is clearly significant. We drew shaded rectangles in the figure to indicate the regions (with generous error bounds) where the slope changes. The lower break occurs at 0.4 J/cm^2 (±50%). The upper break occurs at 3 J/cm^2 (±50%). Our predicted fluences for the onset of

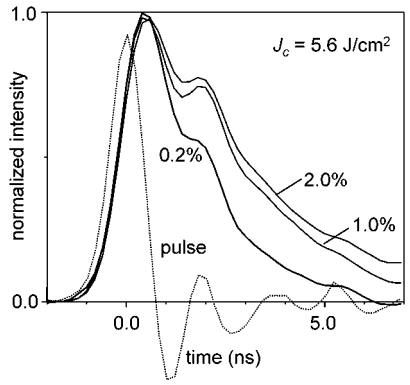

Figure 8. Time-dependent emission from flash-heated ALEX/NC. The data labeled "pulse" are the apparatus response to a 30 ps pulse. At a fixed fluence of $J_c = 5.6$ J/cm^2, the concentration threshold for total ignition is 0.5% ALEX. The decay time constant is 2.0 ($\pm$0.5) ns with 0.2% ALEX, where hot spots ignite and extinguish without totally igniting the sample. The decay are constants are 3.5 ($\pm$0.5) ns with 1.0% and 2.0% ALEX, where the sample is totally ignited.

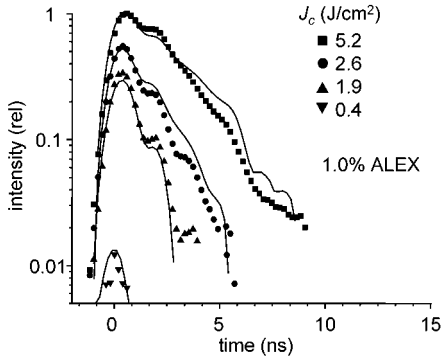

Figure 9. Time-resolved emission from a 1.0% ALEX sample. The fitted curves are numerical convolutions of the apparatus response and exponential functions.

vaporization ($J_c = 1.8$ J/cm^2) and for the melting transition ($J_c = 0.4$ J/cm^2) are found in the upper and lower shaded regions, respectively.

C. Time-Resolved Emission. The time dependence of the emission (effectively integrated over the 350−820 nm range) is shown in Figures 8 and 9. The curve in Figure 8 denoted "pulse" is a measurement of the apparatus response using a 30 ps laser pulse. The apparatus impulse response is highly reproducible, with a fwhm of ~1 ns and significant ringing. Despite the ringing, we could characterize each decay reasonably well by fitting it with the numerical convolution of the apparatus response and an exponential function (see Figure 9) with time constant τ_{exp}. The use of an exponential function is not meant to rule out the possibility that the decays are nonexponential or multiexponential. The estimated error in τ_{exp} judged from quality of fit was $\pm$0.5 ns.

At a fixed higher fluence $J_c = 5.6$ J/cm^2, the emission lifetimes were measured (Figure 8) above and below the concentration threshold (0.5% ALEX) for complete ignition (see the discussion of Figure 4). Below this concentration threshold (e.g., 0.2% ALEX) the lifetime was $\tau_{exp} = 2.0$ ns. Above this threshold (e.g., 1.0% and 2.0%) $\tau_{exp} = 3.5$ ns. At fixed concentration of 1% ALEX, the lifetimes were measured (Figure 9) above and below the fluence threshold for complete ignition (between 1.3 and 1.9 J/cm^2; see the discussion of Figure 5). At $J_c = 0.4$ J/cm^2, where there is no evidence for Al or AlO emission, the ALEX particles just heat and cool without much chemistry, and the fitted curve in Figure 9 gives $\tau_{exp} < 0.7$ ns.

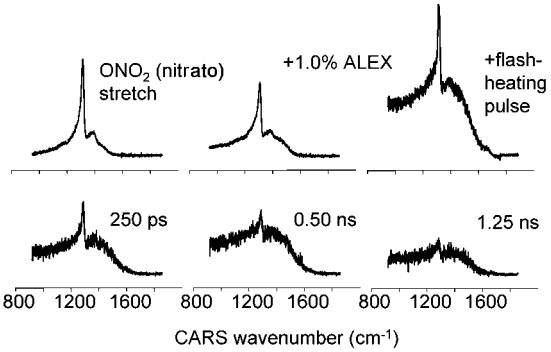

Figure 10. Broadband multiplex CARS spectra in the vicinity of the symmetric ONO_2 stretching transition (the sharp feature on the nonresonant background). Adding ALEX (+ 1% ALEX) decreases the signal level. The flash-heating pulse causes the sample to ignite, and an optical background appears along with CARS. As time progresses, nitro consumption is observed via the intensity decline of the ONO_2 (nitrato) peak.

Increasing the fluence to $J_c = 1.9$ J/cm^2 causes the lifetime to increase to $\tau_{exp} = 2.0$ ns. At $J_c = 2.6$ J/cm^2, $\tau_{exp} = 3.0$ ns and at $J_c = 5.6$ J/cm^2, $\tau_{exp} = 3.5$ ns.

D. CARS of ONO_2 (Nitrato) Symmetric Stretching. Figure 10 shows representative CARS spectra from NC in the ONO_2 (nitrato) symmetric stretching region. The decline of nitrato intensity is used to infer nitro consumption within the sample. The observation window is centered near 1300 cm^{-1} with a 350 cm^{-1} width. The shape of this window is determined by the broadband dye laser's output spectrum.[41] A spectrum of 3.3 μm NC has an excellent signal-to-noise ratio of about 100:1. Adding 1% ALEX attenuates the probe pulses and increases the scattered light. The burst of emission caused by the flash-heating pulse adds an optical background. The fluctuations in this background are the greatest source of noise in the measurement. The background intensity is independent of the time delay between the flash-heating pulse and the CARS pulses because the CCD detector time-integrates the signal. As the delay time after the flash-heating pulse is increased, the nitrato intensity decreases. This intensity decrease is not caused by a loss of optical transparency in the sample because nonresonant CARS signals show no such decrease. The nitrato transition does not appear significantly broadened up to 0.5 ns, which is about the longest delay possible for a reliable line width determination. The lack of broadening indicates the unconsumed oxidizer temperature is well below the thousands of degrees associated with ignition.[7]

The CARS data were used to determine the time-dependent nitro survival fraction $S(t)$. In CARS spectroscopy, the concentration is proportional to the *square root* of the intensity.[47] We have to account for both the square-root dependence and the emission background. Let $I_{CARS}(t)$ represent the CARS signal at the wavenumber of the nitrato transition peak. Then $I_{CARS}(t<0)$ represents the nitrato CARS signal prior to flash-heating plus the emission background. The survival fraction is given by

$$S(t) = \frac{\sqrt{I_{CARS}(t)} - \sqrt{I_{CARS}(t<0)}}{\sqrt{I_{CARS}(t<0)}} \qquad (4)$$

Owing to the background fluctuations and the square-root dependence, the survival fraction measurements are estimated to have an accuracy and sensitivity of about $\pm$10%.

Figure 11 shows the fluence dependence of $S(t)$ in the 0−7 ns time range, with 1.0% ALEX. A few data points were

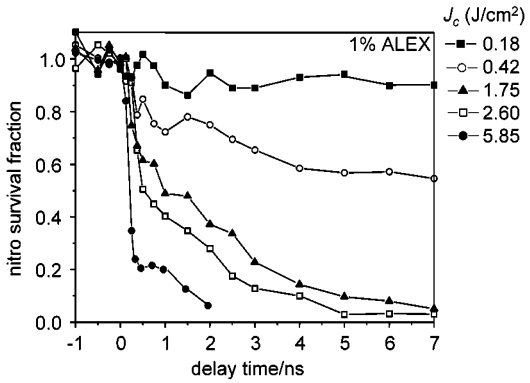

Figure 11. Nitro survival fraction $S(t)$ versus time at various laser fluences, for a sample containing 1.0% ALEX. The $S(t)$ decay occurs in two parts whose relative amplitudes depend on fluence. The time constants for the two processes, which do not depend strongly on fluence, are ~300 ps and ~2 ns. The faster process is identified with hot spot initiation and the slower with initiation propagation.

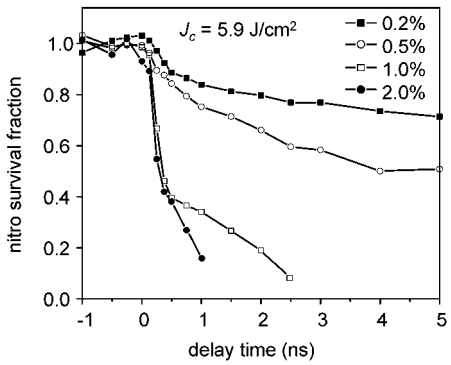

Figure 12. Nitro survival fraction $S(t)$ versus time, for different ALEX concentrations at a fluence of $J_c = 5.9$ J/cm^2. At this fluence, Figure 4 shows the concentration threshold for total ignition is about 0.5% ALEX.

obtained out to 20 ns and show that $S(t)$ does not change significantly in the 7−20 ns time range. Recall that Figure 5 shows the threshold fluence for complete ignition with 1.0% ALEX is in the 1.3−1.9 J/cm^2 range. At $J_c = 0.18$ J/cm^2, there appears to be a small amount of nitro loss occurring within the first few nanoseconds that is near our detection limit. Two-step nitro consumption is observed at all higher fluences. The amplitude of the faster subnanosecond part increases with increasing fluence until it is more than 90% at the highest fluence. It is difficult to be precise about the decay time constants, but it is remarkable that the two time constants hardly change with fluence, considering that the fluence ranges over an order of magnitude, and the predicted ALEX temperatures range from a few hundred to a few thousand degrees. Thus it is possible to describe nitro consumption as occurring in a 300 ps phase and a 2 ns phase, whose amplitudes are strongly fluence dependent.

Figure 12 shows the ALEX concentration dependence of $S(t)$ at a fixed higher fluence $J_c = 5.9$ J/cm^2. Recall that Figure 4 shows the concentration threshold for complete ignition at this fluence is a bit above 0.5%. As in Figure 11, $S(t)$ always shows a 300 ps part and a 2 ns part. The amplitude of the 300 ps decay increases with increasing ALEX concentration at fixed fluence. Below the concentration threshold of 0.5%, nitro consumption does not become complete, even at longer times. Above this threshold, $S(t)$ drops to nearly zero in less than 2 ns.

5. Discussion

In this section we first critically examine the temperature estimates from section 2, and then return to the themes of initiation, ignition, hot spots, propagation, and energy release introduced in section 1.

A. Temperature Calculations. Our thermal diffusion calculations of the Al particle temperature immediately after the 100 ps flash-heating pulse assumed 100 nm particles with the reflectivity of bare oxidized Al and no heat generated by chemical reactions during the pulse. A significant error could occur if the nanoparticle reflectivity differed from bulk Al. A secondary issue is the size distribution and aggregate nature of the ALEX particles, which ought to result in a spread of particle temperatures. Particles much larger than 100 nm, or smaller particles in the shadow of larger particles might be colder than predicted. Mie scattering[36] from the nanoparticle suspension may produce regions of locally enhanced electric fields where the particles will be hotter.

Our temperature estimates are supported by the following. On the basis of ignition[5] and slow heating[9] studies, we would expect Al particles to first become activated near T_m. However, if the reaction with oxidizer near T_m was slower than the (roughly nanosecond) time for the particles to cool below T_m, little chemistry would be observed. On the basis of laser ablation studies,[43] highly energetic nanosecond time scale reactions would not be expected until T_{vap}. The onset of scattered ignition reactions (Figure 5) and the onset of nitro consumption (Figure 11) occur near the putative melting threshold $J_c = 0.4$ J/cm^2. A break in slope in the intensity versus fluence curve (Figure 7b) is also observed near $J_c = 0.4$ J/cm^2. The spectrum at this fluence (Figure 7) has a low intensity, with no sign of Al atom or AlO emission. Some light emission (Figure 7) and nitro consumption (Figure 11) is observed at fluences as low as $J_c = 0.2$ J/cm^2, which we attribute to the occasional hotter Al nanoparticle.

Near the putative vaporization transition $J_c = 1.8$ J/cm^2, we start to see Al atom and AlO emission (Figure 7a) and the second break in slope in the emission versus fluence curve (Figure 7b). This fluence region is also where we first start to see substantial fast consumption of oxidizer (Figure 11) and complete ignition of the heated region (for 1% ALEX concentration, Figure 5). A small amount of Al emission is observed at fluences as low as $J_c = 1.3$ J/cm^2 (Figure 7), but once again we associate that with the occasional hotter Al nanoparticle.

Taken together, these observations suggest that our predictions of the melting and vaporization transitions are reasonably accurate, provided we use broad confidence limits (±50%, the widths of the shaded regions in Figure 7b) and keep in mind the temperature distribution caused by the aggregate structure of ALEX.

B. Initiation. The best indicators of initiation are the nitro consumption CARS experiments (Figures 11 and 12) and the microscope images (Figures 4 and 5). ALEX particles are predicted to range from slightly vaporized to totally vaporized with J_c ranging between 1.8 and 8 J/cm^2. The Al vapor will react with an equivalent amount of nearby NC. At the lower end of this fluence range, we would expect hot spots to be smaller and more likely to extinguish quickly. At the higher end, the hot spots will be larger and could possibly grow before extinguishing—to a maximum diameter of a few microns before being quenched by the substrate. Looking at the 300 ps decay in Figures 11 and 12, we see that the amplitude increases with increasing laser fluence at constant ALEX concentration, and the amplitude increases with increasing ALEX concentration

at constant laser fluence. For these reasons, we associate the 300 ps decay with initiation near an ALEX particle leading to hot spot formation.

The slower 2 ns part of the decay thereby represents nitro consumption caused by the ignition reaction propagation. A delay due to propagation into the NC between the ALEX particles, in a sea of hot ALEX particles, will be most noticeable with large growing hot spots spaced far apart, but the propagation delay will be inconsequential when the average spacing between hot spots is smaller than or comparable to their diameters. The ignition propagation reaction depends on chemical dynamic factors, and in addition it depends a great deal on geometry. It ought to be possible to develop models for ignition propagation, but the problematic structure of the ALEX aggregates is a confounding issue. We would have to deal with a distribution of size and shape for the hot spots, and the spatial distribution of these hot spots will be quite complicated. To better deal with this problem, we are presently working on developing samples with monodisperse nonaggregated metal nanoparticles.

C. Ignition. The indicators of ignition are the intense bursts of light emitted after flash-heating (Figures 6−9) and the microscope images (Figures 4 and 5). Following the initiation discussion above, ignition ought to proceed in two stages, hot spot ignition near an ALEX aggregate, and ignition propagation into the regions between hot spots.

To separate the effects of ignition from ignition propagation, we should compare results from lower fluences or lower ALEX concentrations where hot spots ignite but do not spread, to higher fluences or higher concentrations where the entire heated region ignites. In Figure 8, the 0.2% ALEX measurement is below the concentration threshold for complete ignition, and it can be fit by an exponential with a ∼2 ns time constant. In Figure 9, the $J_c = 1.9$ J/cm^2 measurement is near the threshold fluence for complete ignition, and the time constant is also ∼2 ns, so ∼2 ns is the time for fast heat and light emission when propagation effects are minimal. The very fast transient associated with the $J_c = 0.4$ J/cm^2 in Figure 9 is explained by noticing it is not a true ignition event, in the sense that the light burst is weak and it lacks Al or AlO features. The subnanosecond emission burst is probably graybody emission, possibly augmented by a small amount of chemiluminescence produced by ALEX heated just above T_m within 100 ps, and which cools back below T_m in less than 1 ns.

In the higher concentration and higher fluence regimes, the emission burst ought to be longer than 2 ns due to reaction propagation effects. Figures 8 and 9 show that at fluences around 5 J/cm^2 with higher concentrations of 1% and 2%, the emission burst lifetime is 3.5 (±0.5 ns). This lengthening of the emission burst due to propagation provides a rough estimate for the ignition propagation time (recognizing that this time ought to depend on concentration and fluence) of 1.5−2 ns, which is comparable to the slower part of the nitro consumption data in Figures 11 and 12.

D. Energy Release. The previous discussion shows that fast energy release occurs in ∼2 ns under conditions where ALEX is vaporized by flash-heating, when propagation effects are minimal. Propagation effects with the concentrations and thin-film geometry used here can evidently add another 1.5−2 ns to this time. In our previous letter[7] on ALEX/NC, we looked only at a single concentration (1% ALEX) with a single fluence (4 J/cm^2), and we used a slower (∼3 ns rise time) detector. We obtained a lifetime for the emission burst of 5 (±2) ns. By using a faster PMT detector, we have made an improved determination of the emission burst lifetime under similar conditions, 3.5 (±0.5) ns. More importantly, as a result of the concentration- and intensity-dependent study, we now see that this 3.5 ns time constant includes a contribution from ignition propagation, so that 2 ns is a better estimate for the fast energy release process.

Even though the improved estimate of 2 ns for the energy release is somewhat faster than the value cited in our earlier letter,[7] it remains quite a bit slower than the 300 ps oxidizer consumption process. Thus the present results are in agreement with the conclusions presented previously. The rate-limiting step in energy release is not activation/depassivation of the metal particles, nor the formation of oxidized Al as indicated by nitro consumption, but rather the release of energy from the hot nascent aluminum oxides. Because the radiative lifetime[45,48] of Al−O in the gas phase is 100−200 ns, the energy release rate is determined mainly by nonradiative relaxation, specifically internal conversion and vibrational cooling. Keep in mind that this conclusion applies only to the high-temperature regime above T_{vap}. Energy release at lower temperatures just above T_m is too slow for us to measure because the flash-heated nanoparticles cool before reacting, and there other processes such as activation/depassivation may be rate-limiting.

The energy release rate is only one of a myriad of factors that influences energetic material performance, and the fastest energy release is not always most desirable. For instance, controlled slower energy release is desirable in solid fuel rocket motors (should not explode!), undersea explosives (better coupling to the slower-moving shock waves in water), and armor-penetrating munitions (should penetrate before exploding). However, one of the key issues in nanoenergetic material development is formulating materials that undergo *self-sustained detonation* as opposed to fast combustion. A self-sustained detonation is a shock front that propagates through a material at constant supersonic velocity, initiating exothermic chemistry as it passes, being driven by work from the rapid expansion of hot gas-phase reaction products behind the front.[49] The 2 ns time constant for energy release is faster than the 10−100 ns time constant deduced for high-performance molecular explosives such as HMX, so it is clearly fast enough for detonation applications.

6. Summary and Conclusion

We have developed a reasonably reliable method for estimating the flash-heating temperature of Al nanoparticles. Approaching the putative melting transition, a small amount of light is emitted that is broad and featureless, and hot ALEX particles cool before much chemistry can occur. Near the putative vaporization transition, an energetic ignition process is observed that is characterized by a nanosecond light burst that includes a continuum peaked near 500 nm plus Al and AlO emission. Microscope images of flash-heated samples show that at lower fluences and lower ALEX concentrations, if ignition is present it is confined to scattered hot spots. At a critical ALEX concentration threshold (that depends on fluence) the reaction propagates into the NC between the hot spots and the entire sample is consumed.

The emission lifetime was found to be ∼2 ns when measured under conditions where ignition occurred but did not propagate very far. Under conditions where the reaction propagated out from the hot spots, the lifetime was increased to 3−3.5 ns. Thus 2 ns is the time for energy release when propagation effects are minimal. The actual energy release time in a real sample could be anything longer than 2 ns, depending on how fast the ignition reaction propagates, which in turn depends on nano-

particle properties, concentrations, and sample dimensions. We are not yet in a position to claim that 2 ns is an intrinsic time constant for energy release in Al/NC, which is determined solely by chemical dynamics, because the ALEX aggregates have a finite size. We need to look in the limit that the size goes to zero. We are working on measuring the energy release rate as a function of decreasing particle size down to 30 nm to help clarify this issue.

The initiation process, as monitored by ultrafast CARS measurements of nitro consumption, shows a faster and a slower part that are associated with hot spot initiation and reaction propagation, respectively. However the ~300 ps time constant for hot spot initiation is significantly slower than the ~2 ns time constant for energy release, proving that the rate-limiting step in energy release with high-temperature initiation is not particle depassivation or oxidizer attack. Instead, the energy release rate is determined by nonradiative relaxation of the hot nascent molecules of oxidized Al.

We have developed the tools needed for real-time probing of reaction initiation, ignition, propagation, hot spot formation, and energy release in nanometric energetic materials. This is a significant step in developing a fundamental understanding of the factors that affect their performance.

Acknowledgment. This material is based upon work supported by the U.S. Army Research Office under award number DAAD19-00-1-0036, the Defense University Research in Nanotechnology (DURINT) program administered by the U.S. Army Research Office under award number DAAD19-01-1-0558, and the Air Force Office of Scientific Research under awards F49620-00-1-0049 and F49620-03-1-0270. Measurements of thin film thickness were carried out in the Center for Microanalysis of Materials, University of Illinois, which is supported by the U.S. Department of Energy under grant DEFG02-91ER45439. We thank the referee for many useful comments.

References and Notes

(1) Fried, L. E.; Manaa, M. R.; Pagoria, P. F.; Simpson, R. L. *Annu. Rev. Mater. Res.* **2001**, *31*, 291.
(2) Tillotson, T. M.; Gash, A. E.; Simpson, R. L.; Hrubesh, L. W.; Satcher, J., J. H.; Poco, J. F. *J. Non Cryst. Solids* **2001**, *2001*, 338.
(3) Politzer, P.; Lane, P.; Grice, M. E. *J. Phys. Chem. A* **2001**, *105*, 7473.
(4) Swihart, M. T.; Catoire, L. *Combust. Flame* **2000**, *121*, 210.
(5) Price, E. W. Combustion of metalized propellants. In *Fundamentals of Solid-Propellant Combustion, Progress in Aeronautics and Astronautics*; Kuo, K., Summerfield, M., Eds.; AIAA: New York, 1984; Vol. 90; p 479.
(6) Armstrong, R. W.; Baschung, B.; Booth, D. W.; Samirant, M. *Nano Lett.* **2003**, *3*, 253.
(7) Wang, S.; Yang, Y.; Sun, Z.; Dlott, D. D. *Chem. Phys. Lett.* **2002**, *368*, 189.
(8) DeSena, J. T.; Kuo, K. K. *J. Propul. Power* **1999**, *15*, 794.
(9) Aumann, C. E.; Skofronick, G. L.; Martin, J. A. *J. Vac. Sci. Technol. B* **1995**, *13*, 1178.
(10) Köhler, J.; Meyer, R. *Explosives*, 4th ed.; VCH Publishers: New York, 1993.
(11) Simpson, R. L.; Urtiew, P. A.; Ornellas, D. L.; Moody, G. L.; Scribner, K. J.; Hoffman, D. M. *Propellants, Explos. Pyrotech.* **1997**, *22*, 249.
(12) Eaton, P. E.; Zhang, M.-X.; Gilardi, R.; Gelber, N.; Iyer, S.; Surapaneni, R. *Propell. Explos. Pyrotech.* **2002**, *27*, 1.
(13) Zhang, M.-X.; Eaton, P. E.; Gilardi, R. *Angew. Chem., Int. Ed.* **2000**, *39*, 401.
(14) Tarver, C. M. *J. Phys. Chem. A* **1997**, *101*, 4845.
(15) Adams, G. F.; Shaw, R. W., Jr. *Annu. Rev. Phys. Chem.* **1992**, *43*, 311.
(16) Chakraborty, D.; Muller, R. P.; Dasgupta, S.; Goddard, W. A., III. *J. Phys. Chem. A* **2001**, *105*, 1302.
(17) Yoo, C. S.; Holmes, N. C.; Souers, P. D. Detonation in shocked homogeneous high explosives. In *Decomposition, Combustion, and Detonation Chemistry of Energetic Materials*; Brill, T. B., Russell, T. P., Tao, W. C., Wardle, R. B., Eds.; Materials Research Society: Pittsburgh, PA, 1996; Vol. 418, p 397.
(18) Yoo, C. S.; Holmes, N. C.; Souers, P. C. *AIP Conf. Proc.* **1996**, *370*, 913.
(19) Yoo, C. S.; Holmes, N. C.; Souers, P. C.; Wu, C. J.; Ree, F. H.; Dick, J. J. *J. Appl. Phys.* **2000**, *88*, 70.
(20) *Gas-Phase Metal Reactions*; Fontijn, A., Ed.; Elsevier: Amsterdam, 1992.
(21) Garland, N. L.; Nelson, H. H. *Chem. Phys. Lett.* **1992**, *191*, 269.
(22) Baschung, B.; Grune, D.; Licht, H. H.; Samirant, M. Combustion phenomena of a solid propellant based on aluminum powder. 5th International Symposium on Special Topics in Chemical Propulsion, Combustion of Energetic Materials, 2000, Stresa, Italy.
(23) Ritter, H.; Braun, S. *Propell. Explos. Pyrotech.* **2001**, *26*, 311.
(24) Parker, L. J.; Ladouceur, H. D.; Russell, T. P. *AIP Conf. Proc.* **2000**, *505*, 941.
(25) Campbell, A. W.; Davis, W. C.; Ramsay, J. B.; Travis, J. R. *Phys. Fluids* **1961**, *4*, 511.
(26) Bowden, F. P.; Yoffe, A. D. *Initiation and Growth of Explosion in Liquids and Solids*; University Press: Cambridge, U.K., 1952.
(27) Bowden, F. P.; Yoffe, A. D. *Fast Reactions in Solids*; Academic Press Inc.: New York, 1958.
(28) Langer, G.; Eisenreich, N. *Propell. Explos. Pyrotech.* **1999**, *24*, 113.
(29) Tarver, C. M.; Chidester, S. K.; Nichols, A. L., III. *J. Phys. Chem.* **1996**, *100*, 5794.
(30) von Allmen, M. *Laser-Beam Interactions with Materials. Physical Principles and Applications*; Springer-Verlag: Berlin, 1987.
(31) Sun, J. M.; Gerstman, B. S. *Phys. Rev. E* **1999**, *59*, 5772.
(32) Siegman, A. E. *Lasers*; University Science Books: Sausalito, CA, 1986.
(33) Yang, Y.; Hambir, S. A.; Dlott, D. D. *Shock Waves* **2002**, *11*, 129.
(34) Hohlfeld, J.; Wellershoff, S.-S.; Güdde, J.; Conrad, U.; Jähnke, V.; Matthias, E. *Chem. Phys.* **2000**, *251*, 237.
(35) *Handbook of Chemistry and Physics*, 81st ed.; Lide, D. R., Ed.; CRC: Cleveland, OH, 1996.
(36) Bohren, C. F.; Huffman, D. R. *Absorption and Scattering of Light by Small Particles*; John Wiley and Sons: New York, 1983.
(37) Lee, I.-Y. S.; Wen, X.; Tolbert, W. A.; Dlott, D. D. *J. Appl. Phys.* **1992**, *72*, 2440.
(38) Hare, D. E.; Franken, J.; Dlott, D. D. *Chem. Phys. Lett.* **1995**, *244*, 224.
(39) Hare, D. E.; Franken, J.; Dlott, D. D. *J. Appl. Phys.* **1995**, *77*, 5950.
(40) Marsh, S. P. *LASL Shock Hugoniot Data*; University of California, Berkeley: Berkeley, CA, 1980.
(41) Hambir, S. A.; Franken, J.; Hare, D. E.; Chronister, E. L.; Baer, B. J.; Dlott, D. D. *J. Appl. Phys.* **1997**, *81*, 2157.
(42) Hare, D. E.; Dlott, D. D. *Appl. Phys. Lett.* **1994**, *64*, 715.
(43) Pangilinan, G. I.; Russell, T. P. *J. Chem. Phys.* **1999**, *111*, 445.
(44) Bescós, B.; Morley, G.; González Ureña, A. *Chem. Phys. Lett.* **1995**, *244*, 407.
(45) Johnson, S. E.; Capelle, G.; Broida, H. P. *J. Chem. Phys.* **1972**, *56*, 663.
(46) Rosenwaks, S.; Steele, R. E.; Broida, H. P. *J. Chem. Phys.* **1975**, *63*, 1963.
(47) Eesley, G. L. *Coherent Raman Spectroscopy*; Pergamon: Oxford, U.K., 1991.
(48) Salzberg, A. P.; Santiago, D. I.; Asmar, F.; Sandoval, D. N.; Weiner, B. R. *Chem. Phys. Lett.* **1991**, *180*, 161.
(49) Zel'dovich, Y. B.; Raiser, Y. P. *Physics of Shock Waves and High-temperature Hydrodynamic Phenomena*; Academic Press: New York, 1966.